

# A Methodology to Establish the Morphology of Ambient Aerosols

Rafael McDonald and Pratim Biswas

*Aerosol and Air Quality Research Laboratory, Environmental Engineering Science,  
Washington University in St. Louis, St. Louis, Missouri*

## ABSTRACT

The morphology of ambient particulate matter (PM) is an important characteristic that seldom is measured and reported. A study was performed to determine the viability of a method to establish the distribution of shapes and the fractal dimensions of aggregates of ambient aerosols. Particles of PM with aerodynamic diameter less than or equal to 2.5  $\mu\text{m}$  ( $\text{PM}_{2.5}$ ) were captured on different days via size-independent electrostatic precipitation at two sites in St. Louis and examined in a scanning electron microscope (SEM). Nonvolatile particles between 0.1 and 2.5  $\mu\text{m}$  were readily identified via SEM. Particle shapes were classified as fibrous, spherical, agglomerated, or "other." A computer program using the nested-squares algorithm was developed and used to determine the fractal dimensions of the aggregates.

More particles were collected at the St. Louis-Midwest Supersite on June 14, 2002, than were collected on the Washington University campus loading dock on May 31, 2002, but the campus samples had a higher percentage of aggregates. On one day of sampling at the Supersite, the aggregate fraction was highest in the morning (14.3% between 7:00 and 9:00 a.m.) and steadily declined during the day (1.3% between 5:00 and 7:00 p.m.). The fractal

dimensions of the aerosols were 1.65 in the morning (7:00–9:00 a.m.), decreased to 1.49 (11:00 a.m.–1:00 p.m.), and then increased to 1.87 (5:00–7:00 p.m.). The results show that the fractal dimension is not a static value and that ambient aerosols are not perfectly spherical.

## INTRODUCTION

Ambient aerosols are of great interest because of their potential role in causing various deleterious health effects.<sup>1–5</sup> There are several characteristics of the ambient particulate matter (PM) that may be responsible for specific health effects. While current ambient PM regulations are based on the mass concentration of particles smaller than an aerodynamic diameter of 2.5 and 10  $\mu\text{m}$ , there may be additional parameters such as particle size, shape, and chemical composition that may be important. A more complete physical representation of the aerosol is by its size distribution, which is important in establishing particle transport, deposition in the respiratory system, and light-scattering properties. While current regulations do not require the determination of size distributions, detailed size distributions down to  $\sim 3$  nm have been measured in many ambient studies, and interesting features have been observed on temporal variations.<sup>6</sup> An important characteristic of the aerosol that is not established routinely is the morphology of the particles.

Many physical characteristics of aerosols are determined by a combination of their size and morphology, yet this second property often is ignored. The morphology of the particles affects the drag force, which, in turn, affects its transport properties. Transport properties would enable the determination of the regions of the lung where the aerosols deposit. Morphology also is important in establishing the light-scattering properties of an aerosol. Many real-time size distribution instruments, such as differential mobility analyzers, measure the mobility equivalent size. There have, however, been few studies relating the mobility equivalent diameter to particle structure.<sup>7,8</sup> An exception is the study by McMurry and Woo,<sup>6</sup> wherein an aerosol mass analyzer was used to

## IMPLICATIONS

The ambient aerosol consists of particles of many different shapes. However, instruments typically measure an equivalent spherical diameter, which may not be sufficient to explain transport and dynamic characteristics. Inaccuracies in these characteristics could result in inaccurate estimations of properties such as respiratory deposition. The determination of the morphology of ambient aerosols is critical if surface area, which has been suggested as one of the prime indicators of potential health effects, has to be established accurately. This paper shows that ambient aerosols are not all spherical, and a methodology has been proposed for its determination. Furthermore, spatial and temporal variations in the morphological characteristics are established that may help elucidate potential sources of the ambient aerosol.

determine accurately the mass of a mobility-classified particle. This then was used to determine the density of spherical particles. An effective density could be determined for ambient agglomerates. Using this, they reported an effective dynamic shape factor for agglomerated aerosols. Morphology also can play an important role in source apportionment or source matching, where it can be used to tell the difference between chemically similar particles that are created by different processes.<sup>9,10</sup> Yet very little is known about the morphology of ambient aerosols, despite the important role it plays in determining the physical characteristics of that aerosol.

The concept of the fractal dimension often has been used to describe agglomerated aerosols,<sup>11-13</sup> but few have used it to describe ambient aerosols. Xiong and Friedlander<sup>14</sup> looked at ultrafine (aerodynamic diameter smaller than 0.1  $\mu\text{m}$ ) ambient aerosols collected on an eight-stage low-pressure impactor and examined them with transmission electron microscopy (TEM). They reported that the two-dimensional fractal dimension increased from 1 to 2 as the number of primary particles increased from 10 to 180. Phoenix aerosols (0.1–2.6  $\mu\text{m}$ ) examined by the same methodology<sup>9</sup> had fractal dimensions ranging from 1.35 to 1.89 but were found to be independent of aerosol size. Dye et al.<sup>15</sup> measured the perimeter and density fractal dimensions of fine urban aerosols (<0.1  $\mu\text{m}$ ) close to and far away from a road, collected on porous carbon films in a cyclone. They found that the average density fractal dimensions were the same in both locations ( $D_f = 1.56$  and 1.57, respectively). Ebert et al.<sup>10</sup> also used impactor sampling to determine the shapes of ambient aerosols by high-resolution scanning electron microscopy (SEM). They classified the particles into 10 categories on the basis of elemental composition and qualitative morphology.

All of the studies used collection methods (impactors and cyclones) that, because of high impaction velocities, may have changed the morphology of the aerosol during collection. This paper describes a method to determine the fractal dimension of aggregated ambient aerosols, using a collection method that is less likely to deform and affect the aerosol morphology, by depositing particles in an electric field. A process of calculating the value of the fractal dimension from electron micrographs is developed. While the primary objective was to describe the experimental and analytical methods used, a comparison between the distributions of particle shape and the associated fractal dimensions of the agglomerates collected in two different locations is illustrated.

## METHODS

### Analytical

**Agglomerate Characterization.** Euclidean geometry cannot be used to describe the complex shapes of many ambient

particles. One approach that has been proposed is the use of a fractal dimension.<sup>11,12,14-18</sup> The fractal dimension relates a physical characteristic (such as volume,  $V$ ) of the object to a characteristic size (length dimension,  $R$ ) of the sample:

$$V = k * R^{D_f} \quad (1)$$

where  $k$  is a proportionality constant. For a particle that is cubical in shape,  $D_f = 3$ ,  $k = 1$ , and  $R$  is the length of a side of the cube, while, for a sphere,  $D_f = 3$ ,  $k = 4\pi/3$ , and  $R$  is the radius. While  $D_f$  is typically an integer for Euclidean shapes, the relationship in eq 1 also holds for non-Euclidian shapes such as agglomerated ambient aerosols, only  $D_f$  is not restricted to integer values. As shown by the previous equation, for any given characteristic size,  $R$ , a larger  $D_f$  corresponds to a larger volume. As such, the larger  $D_f$  is, the higher the "density" of the measured characteristic. In the case of aerosols, a higher  $D_f$  corresponds to a more compact (dense) structure. More detailed explanations of the fractal dimension are given elsewhere.<sup>9,11,15,17-20</sup>

In this paper, the fractal dimension that will be used to describe aggregates is

$$N_p = k \left( \frac{R_g}{a} \right)^{D_f} \quad (2)$$

where  $N_p$  is the number of primary particles in the aggregate,  $k$  is a dimensionless prefactor,  $R_g$  is the radius of gyration,  $a$  is the primary particle radius, and  $D_f$  is the fractal dimension. For a given radius of gyration, the higher the fractal dimension, the higher is the number of primary particles in an agglomerate, thus resulting in a higher number density (because  $R_g$  is fixed). Assuming that the primary particles in the aggregate are spherical, the maximum surface area ( $A_{\text{max}}$ ) can be calculated using eq 2 to yield

$$A_{\text{max}} = 4\pi k R_g^{D_f} a^{2-D_f} \quad (3)$$

If the agglomerates are partially sintered, as encountered in some combustion source exhausts,<sup>21,22</sup> the surface area would be less than that estimated from eq 3. However, if aggregate formation occurs in the atmosphere or takes place at temperatures where sintering is slower than collisional time scales,<sup>23</sup> eq 3 would provide a good estimate of the surface area.

**$D_f$  Determination.** Fractal dimensions can be calculated based on the perimeter or the density. The perimeter fractal dimension (PFD)<sup>15,18</sup> describes the roughness of

the aggregate, while the density fractal dimension<sup>9,14</sup> describes the space-filling characteristics of the aggregate.

A macro available with the computer program Scion Image<sup>24</sup> was used to calculate the PFD. The program draws a grid on the two-dimensional image of the aggregate. It counts the number of squares through which the perimeter passes. The size of the squares in the grid then is changed, and the number of boxes through which the perimeter passes is counted again. This process is repeated several times, generating a list of box sizes and the number of boxes that contain part of the particle perimeter. The slope of the curve plotting the logarithm of the box size versus the logarithm of the number of boxes is the PFD.

Two programs were used to calculate the density fractal dimension. A Matlab program<sup>25</sup> developed in the Aerosol and Air Quality Research Laboratory was used first. The user first is required to click on the center of every particle on a picture of the agglomerate and then on the edges of a primary particle (to determine the primary particle diameter). Starting from the center of mass, circles of increasing size are drawn on the aggregates. The number of primary particles contained inside each circle is calculated, generating a list of radii and number of primary particles. A log-log plot of eq 2 is generated, the slope of which is the density fractal dimension. The major issue with the program is that it assumes that every primary particle is perfectly spherical and exactly the same size. The second issue is that the program did not account for the problem of length scales. It is important to note that the aggregates are fractal only on a certain length scale.<sup>23</sup> If that length scale is too small, then all of the circles are completely filled. On the other hand, there is a point where increasing the circle size does not increase the number of black pixels. These sizes are dependent upon the mass distribution within the aggregate. This program did not deal with the length scales issue, calculating the slope of the log-log curve using all the data points, including those outside the linear region.

To solve some of these problems, a customized macro was written using the imaging software, ImageJ.<sup>26</sup> The cumulative-intersection method was used, which also is known as the nested squares method.<sup>14,15,20</sup> To solve the primary particle problem, pixels, rather than individual primary particles, were used to calculate the density fractal dimension. First, the image (Figure 1a) of the agglomerate was threshed. Threshing is an automated procedure that converts the image into a black and white image, where black pixels represent part of the particle and white pixels represent everything else (not part of the agglomerate). Boxes of increasing size are then drawn on the image, centered on the particle's center of mass (Figure 1b). The number of black pixels inside each box is

calculated, which generates a list of box sizes and number of pixels. To solve the problem of length scales, data points outside the linear region of the log-log plot are excluded. While discarding data points is not desirable, it is a relatively simple way to eliminate the problem of length scales.<sup>15</sup> The fractal dimension of the aggregate is then calculated as the slope of the linear portion of the log-log curve (Figure 1c). If more than 40% of the data points are outside the linear region, the aggregate is classified as a nonfractal aggregate and is not used in the calculation of the fractal dimension of the entire sample. Orientation effects were not considered during analysis, because they have been found to account for less than 5% variation.<sup>15</sup>

All three programs were used to calculate the respective fractal dimensions of 13 ambient aggregates. The ImageJ macro developed in this work was found to be the most effective. Hence, the density fractal dimension then was calculated for all the other samples using the ImageJ macro. The fractal dimension of the sample then was calculated as the arithmetic mean of all of the aggregates in that sample.

## Experimental

**Sample Collection.** Figure 2 is a diagram of the system used to sample the ambient aerosols. The PM with aerodynamic diameter less than or equal to 10  $\mu\text{m}$  ( $\text{PM}_{10}$ ) inlet of a tapered element oscillating microbalance (TEOM—Rupprecht and Patashnick, Model #1400a) was followed by a PM with aerodynamic diameter less than or equal to 2.5  $\mu\text{m}$  ( $\text{PM}_{2.5}$ ) cyclone to pre-classify the ambient aerosol by impaction. An electrostatic aerosol sampler (EAS; TSI, Model #3100A) was connected to the bypass flow of the TEOM. Particles were collected in the EAS on Lacey Support Film TEM grids (Ted Pella, Model #01883), which were changed every 2 hr between 7:00 a.m. and 7:00 p.m. local time. A total of  $\sim 4$  m of 3/8-in. Teflon tubing was used for transporting the aerosol from the 2.5  $\mu\text{m}$  cutoff to the EAS. Losses caused by gravitational settling and diffusion to the tube walls were calculated to be less than 1%.<sup>27</sup> Losses caused by electrostatic forces in the Teflon tubing, however, can be quite high<sup>28</sup> (as high as 30% loss for particles with a Boltzmann distribution).

To achieve the 2.5- $\mu\text{m}$  cutoff, the TEOM head requires 16.68 L/min of flow. The microbalance, however, only requires 3.01 L/min, leaving 13.67 L/min as bypass flow. The EAS was inserted in the bypass flow path. For the EAS, 13.67 L/min is too high of a flow rate, so a second bypass was put around the EAS, which recombined with the 4 L/min EAS flow after the sample was collected. Flow rates are maintained by the TEOM control unit, which operates two flow controllers, one for the bypass flow, and one for the main flow.

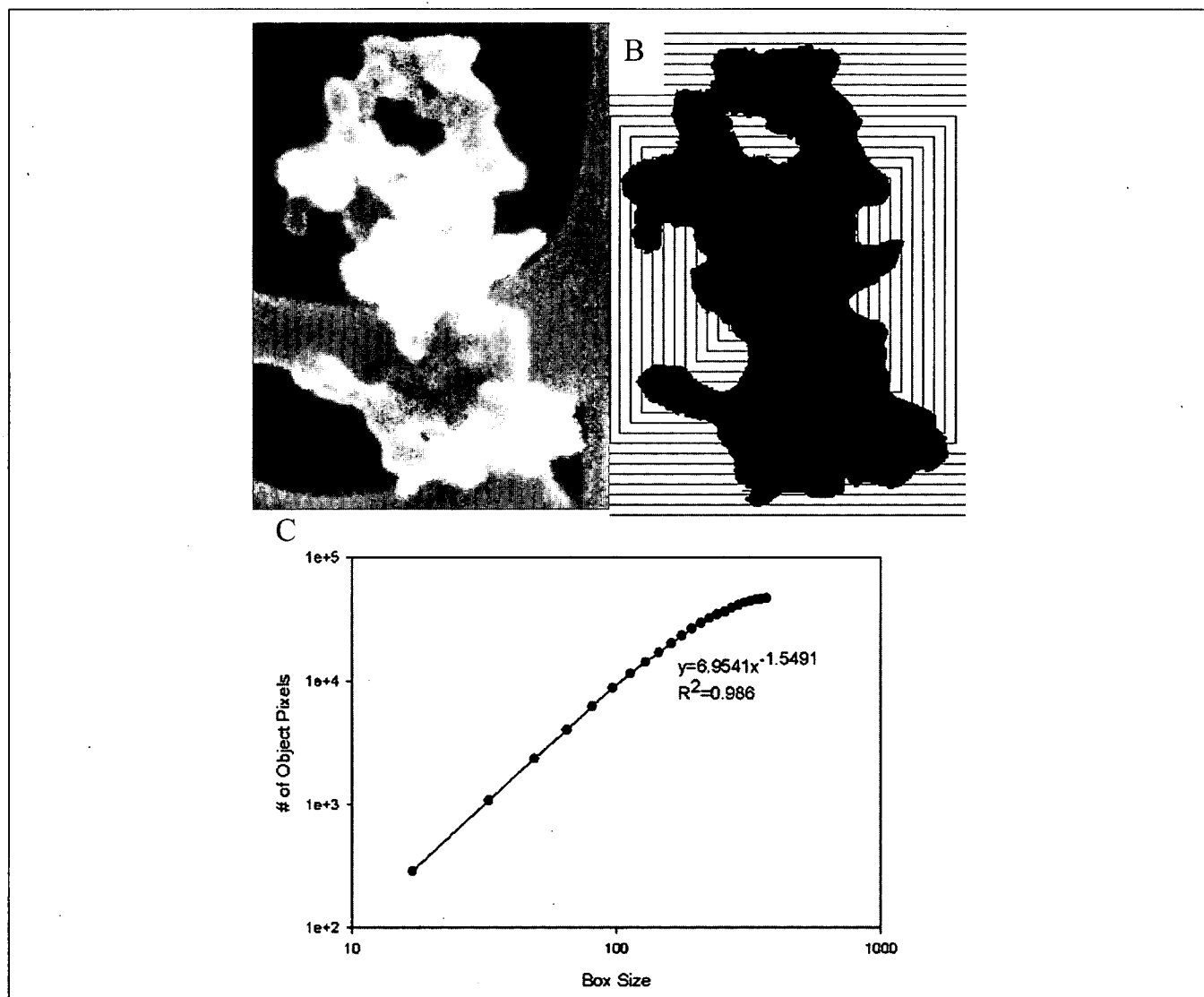


**Figure 1.** The three steps to determine fractal dimension. (A) The micrograph is scanned; (B) the thresholded image has concentric boxes drawn on it and the number of "on" pixels is counted in each box; (C) a log-log plot of  $N$  vs.  $l$ , where the slope of the best linear fit is the fractal dimension.

The differing flow rates and the use of the  $t$  junction immediately before the EAS contribute to anisokinetic sampling conditions. However, for Stokes numbers less than 0.01, particle losses by inertia are negligible,<sup>29</sup> and the concentration of particles coming into the junction is the same as the particles leaving the junction. At the flow rates used, particles less than  $2.3 \mu\text{m}$  indeed have a Stokes number less than 0.01. Because we were using a  $2.5 \mu\text{m}$  cutoff, only particles between  $2.3$  and  $2.5 \mu\text{m}$  would be affected by the anisokinetic conditions. The geometry of the system would have favored a higher concentration of particles of this size entering the EAS. Because less than 1% (based on number) of the particles viewed were greater than  $1 \mu\text{m}$ , however, the anisokinetic conditions did not bias the sampling.

The EAS uses electrostatic forces to cause a deviation in the path of the particles as they pass through the

sampler. Particles enter the EAS and pass through the charging section, where they are charged by a  $+3500 \text{ V}$  unipolar corona discharge. The particles then pass to the sampling section, where they are exposed to a square-wave (0 to  $+4200 \text{ V}$ ) voltage on a top plate and ground on the collection plate. When the voltage is off, particles of all sizes enter the chamber and randomly mix. When the voltage is applied, particles of all sizes deposit in the same area, eliminating size bias and allowing for the random collection of particles.<sup>30</sup> The EAS can collect particles efficiently in the  $0.02$ – $10 \mu\text{m}$  aerodynamic diameter range. The collection efficiency of the EAS is a weak function of size (70–80% for particles  $0.1$ – $1 \mu\text{m}$ ).<sup>31</sup>

The sampling section is small, so the particles do not reach high velocities perpendicular to the sampling area as they impact the TEM grid, unlike high-impaction velocity conditions encountered in impactors. With a

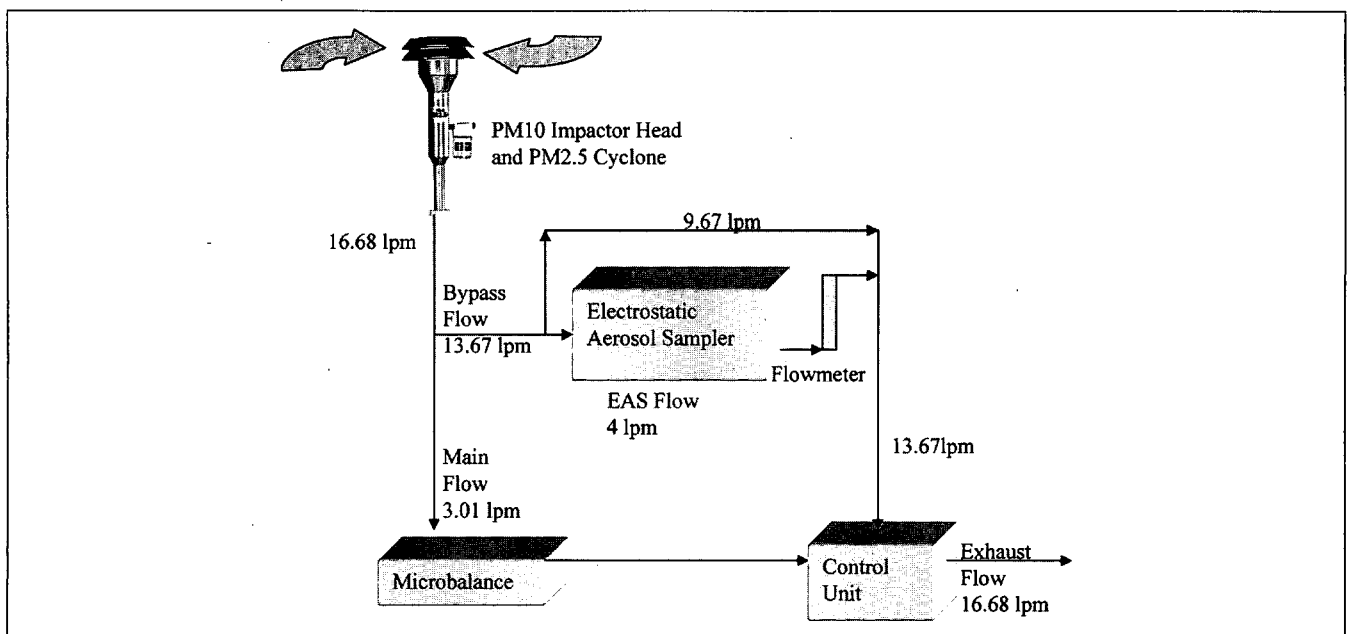


**Figure 2.** Sampling system used to collect particles for morphology determination.

smaller impaction velocity than that experienced in a cyclone or impactor, the forces that the particles experience are smaller, leading to a lower likelihood that the particle will deform plastically upon collection. In a study of diesel soots, aggregate sizes and shapes were found to be the same when measured in situ and via electrostatic means.<sup>16</sup> The identical results indicate that electrostatic collection methods and electromicroscopic analysis do not alter the aggregate morphology.

On Friday, May 31, 2002, samples were collected from a bridge over Throop Drive, close to a loading dock on the campus of Washington University in St. Louis (WUSTL) between 3:00 and 5:00 p.m. At the WUSTL location, a pump was connected directly to the EAS. The lack of a size cutoff allowed particles larger than 2.5  $\mu\text{m}$  to enter the sampling chamber, but they were not included in microscopic analysis for consistency in comparisons with the TEOM-sampled aerosols. The bridge over Throop Drive is  $\sim 5$  m above the road, 20 m from a loading dock, and, on the day sampling was performed,  $\sim 100$  m from some heavy building construction. Throop Drive is an access road, and traffic on it is light, although trucks frequently park at the loading dock. The wind was light that day; however, wind speed and wind direction were not recorded.

On Friday, June 14, 2002, samples were collected at the St. Louis-Midwest Supersite (Supersite), in East St. Louis, IL. The St. Louis Supersite core monitoring location is collocated with the Illinois Environmental Protection Agency (EPA) "East St. Louis RAPS Site" (38.6122N,  $-90.16028$ W) at 13th and Tudor Streets, East St. Louis (IL). Samples were taken between 7:00 a.m. and 7:00 p.m.

The site is located 2 km east of the Mississippi River, which separates East St. Louis (IL) from the City of St. Louis (MO) and is 3 km east of the City of St. Louis' Central Business District (CBD). Interstate 55/64/70 lies  $\sim 1$  km to the west; this highway leads to the Poplar Street Bridge, one of the major routes across the Mississippi River in the St. Louis area. At the microscale level, the site is straddled by freeway on/off ramps with relatively little traffic (nominally  $<10$  cars/min during rush hour). The immediate neighborhood is mixed use (primarily residential, some light commercial) with relatively low population density. This site was chosen because of the pre-existing ambient air-sampling infrastructure. The inlet to the apparatus was  $\sim 5$  m above the ground, and the flow was directed indoors to the TEOM. Tubing from the sampler to the EAS was  $\sim 4$  m long, corresponding to small diffusional losses (0–0.7%) based on diffusional loss calculations described in Hinds.<sup>29</sup> Wind direction was steady (northwest) and parallel to the highway, so the wind did not pass over the highway on the way to the sampler.

**Sample Analysis.** The TEM grids were analyzed for particles in an SEM (Hitachi S4500). Nonvolatile particles between 0.1 and 2.5  $\mu\text{m}$  were readily identified via the SEM. Particles smaller than 0.1  $\mu\text{m}$  could not be resolved adequately for analysis with this SEM. Individual particles were examined as they were encountered in straight-line tracks across the TEM grid. As such, the selection of particles was based on the random distribution of particles on the TEM grid. Total particle count, aerosol shape, and fractal dimensions were determined for each sample.

Only nonvolatile particles were analyzed, because the SEM operates under vacuum conditions. Additionally, anywhere between 1 and 5% of the particles that did not volatilize under vacuum did evaporate when subjected to the electron beam (10 kV). These particles tended to be crystalline in structure and also could not be included in the analysis. Ebert et al.<sup>19</sup> have viewed hygroscopic particles in an environmental SEM (ESEM) and were able to keep volatilization to a minimum.

Charging of the particles by the electron beam can cause the particles to change shape. Most frequently, the dendritic structure of the aggregate would collapse in on itself, resulting in a more compact shape. To keep charging effects to a minimum, a relatively low accelerating voltage of 10 kV was used. Nonetheless, charging was observed in less than 5% of the aggregates encountered. Because the resultant morphology was different than that which the particle had when collected, these collapsed aggregates were not included in the analysis.

Each particle viewed was put into one of four categories based on its two-dimensional projection. Particles comprised of multiple smaller spherical primary particles were classified as aggregates (Figures 3a and 3b). Particles with circular or close-to-circular shapes were classified as spherical (Figures 3c and 3d). Particles with both only one dominant line of orientation and a relatively high aspect ratio (greater than  $\sim 3$ ) were classified as fibrous (Figures 3e and 3f). Particles that did not meet any of the previous criteria were placed in the "other" category (Figures 3g and 3h). For each sample, 50–100 particles were analyzed. In some cases, a sufficient number of agglomerated particles was not detected. In these cases, viewing ceased after four TEM grid squares (1 square  $\sim 4000 \mu\text{m}^2$  surface area) were examined. A micrograph was taken of each aggregate particle.

## RESULTS AND DISCUSSION

Using the procedures outlined, several samples were collected and viewed in the electron microscope. Key details and results of the samplings are listed in Table 1. Sample agglomerates are illustrated in Figure 4.

### Fractal Dimension Method Selection

The different methods described earlier were used to calculate the PDF and density fractal dimensions for 13 selected aggregates that represented a range of shapes of agglomerated particles. Figure 5 shows the results of the comparisons. For the 13 aggregates tested with this method, the macro to determine the PFD consistently determined fractal dimensions between 1.66 and 1.83. The arithmetic average was 1.78, with a standard deviation (SD) of 0.04. The density fractal dimension

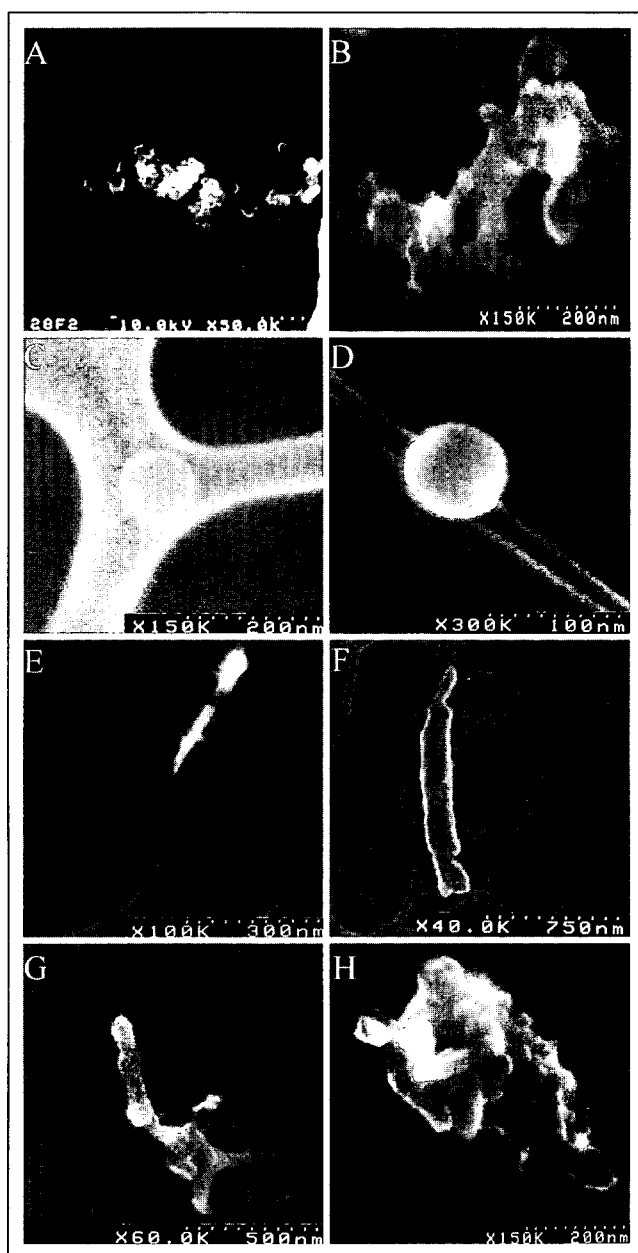


**Figure 3.** Examples of each of the four shape categories of particles; (A, B) aggregated; (C, D) spherical; (E, F) fibrous; and (G, H) other.

calculated with the Matlab Program yielded an average value of 1.61, with an SD of 0.21. The program developed as part of this work yielded density fractal dimensions in the range between 1.39 and 1.89. The average for the same 13 particles was 1.69 with an SD of 0.20. The ImageJ algorithm developed in this study was chosen to calculate the two-dimensional density fractal dimension for all of the particles. The ImageJ program gave similar average values and was more time-intensive than the Matlab program, but it had fewer limitations and problems, as outlined in the Methods section, better reproducibility, and could compensate for length scale issues.

**Table 1.** Overall number and aggregate composition of samples taken at the WUSTL and St. Louis–Midwest Supersite locations.

Sample	Time	Total	Fibrous		Spherical		Agglomerate		Other			
			#	%	#	%	#	%	$D_g$	#	%	
WUSTL May 31, 2002	20A	15:00–17:00	35	9	26%	6	17%	7	20%	1.65	13	37%
	20B	15:00–17:00	33	3	9%	4	12%	9	27%		17	52%
	Average*		34	6	18%	5	15%	8	24%	$1.65 \pm 0.15$	15	44%
Supersite June 14, 2002	23A	7:00–9:00	119	21	18%	16	13%	17	14%	1.65	65	55%
	23B	9:00–11:00	100	18	18%	25	25%	12	12%	1.49	45	45%
	23C	11:00–13:00	85	16	19%	17	20%	10	12%	1.42	42	49%
	23D	13:00–17:00	78	16	21%	13	17%	6	8%	1.53	43	55%
	23E	15:00–17:00	67	17	25%	3	4%	2	3%	1.53	45	67%
	23F	17:00–19:00	65	15	23%	9	14%	1	2%	1.87	40	62%
	Average*		86	17	20%	14	16%	8	9%	$1.57 \pm 0.21$	47	54%

\*Average calculated as the arithmetic average between samples.

### Site Comparisons

Table 1 shows the sampling details and results from both sampling sites. The concentration of particles at the Supersite was more than twice that at the WUSTL location. On average, the numbers of aggregates collected at the

two sites were similar; however, the WUSTL site had a statistically higher fraction of aggregates and a slightly lower fraction of “other” particles. The higher fraction of aggregates at the WUSTL site is because of the proximity to a loading dock where trucks were constantly pulling in and out; and it is known that truck diesel engine emissions are enriched in agglomerates. Both sites had similar fractions of spherical and fibrous particles (Figure 6). Though the WUSTL location had a larger fraction of aggregates, the aggregates at the two sites did not have statistically different fractal dimensions ( $1.65 \pm 0.15$  and  $1.57 \pm 0.21$ , respectively).

A temporal distribution of the particles by number and shape also was established at the Supersite, and the results are plotted in Figure 7a. The absolute number of particles was highest in the morning and steadily decreased as the day went on, with a slight increase in the evening. The drop in absolute number of particles is most likely caused by the change in air parcel exchange rate that occurs during the day. The morning rush hour is a time of high emissions, from both automobiles and trucks. During this time, the mixing height is shallow, and so the concentration of  $PM_{2.5}$  is high. During the evening rush hour, emissions may be high again, but the larger mixing volume leads to a lower concentration of particles. Other meteorological parameters, such as wind speed and wind direction, as well as emissions from non-traffic sources, also may have caused the observed change. Figure 7b is a plot of the variation of the fraction of shape with time of day. Each category has its own dependence with time, and they do not necessarily follow the same pattern as the total concentration illustrated in Figure 7a. The largest fraction of particles in category “other” does indeed follow the “U”-shaped curve as the total number concentration variation, and the same reasoning

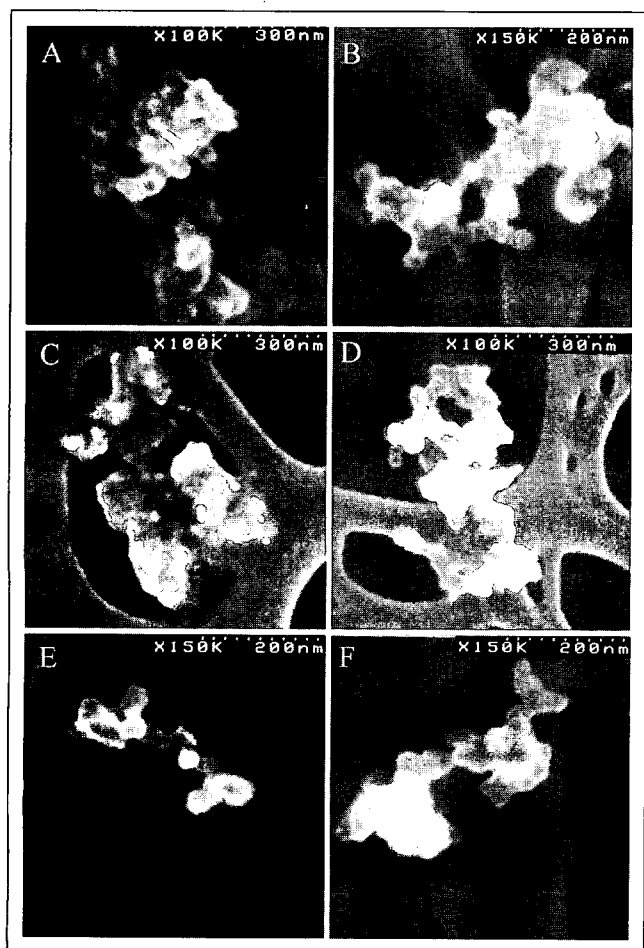


**Figure 4.** Micrographs of aggregates collected at WUSTL and the Supersite. The webbing behind the particles is part of the TEM grid.

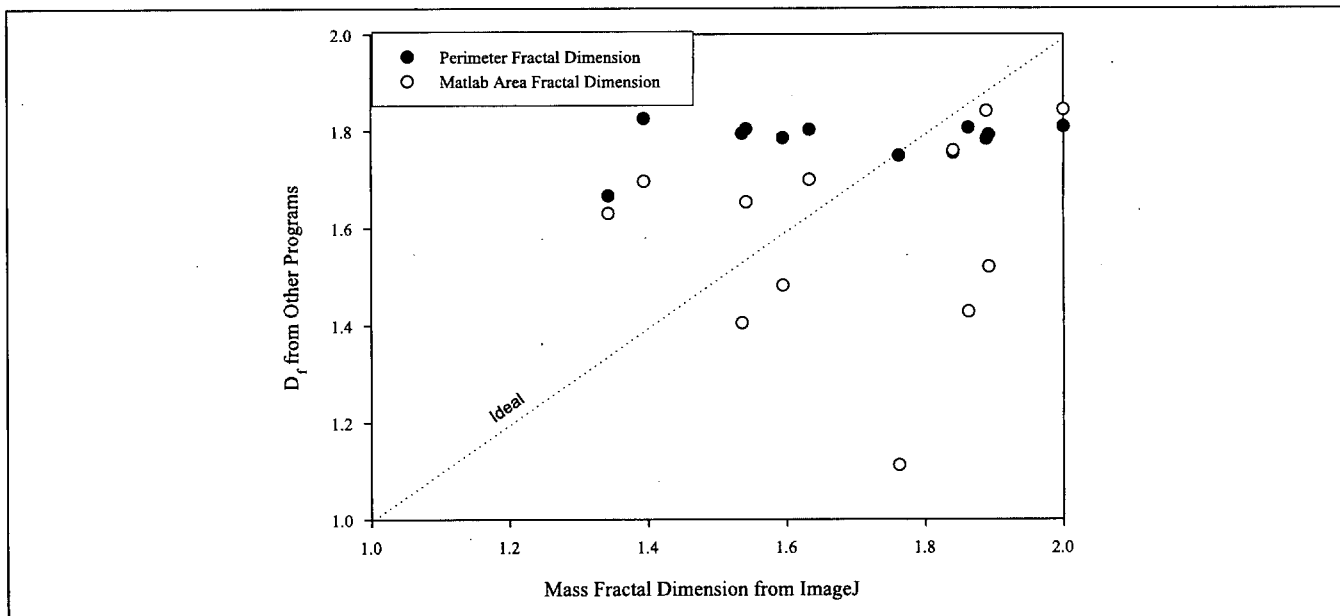


**Figure 5.** Comparison of density fractal dimension calculated with ImageJ (this work) to the density fractal dimension calculated by the AAQRL Matlab program. Also shown is the perimeter fractal dimension calculated by the Scion Image Program.

described previously may be valid. However, more complex effects are at play for the other shape category particles, rather than just a dilution effect because of the variation of the mixing heights. One reason could be that the different shaped particles come from different sources and are emitted at different times and, thus, each has their own unique time dependencies. It is interesting to note that the fraction of both spherical and agglomerated particles tends to decrease at the Supersite—and this is because of a complex dependence on a number of factors, such as wind patterns, traffic patterns, and other variables. Discerning the exact reasons for this variation was beyond the scope of this paper.

Fractal dimensions also were analyzed for each Supersite sample, giving a temporal profile for the day. The 48

aggregates collected had fractal dimensions between 1.4 and 1.7, except for the period of time from 5:00 to 7:00 p.m. (Figure 8). A single-factor analysis of variance (ANOVA) reveals that the fractal dimensions calculated at these different times are different ( $p = 0.07$ ). The low  $p$  value determined by the single-factor ANOVA analysis reveals that the fractal dimension did change with time. If one assumes that traffic is primarily dominated by automobiles in the morning and trucks in the late morning and early afternoon, then the dual roles of automobile and truck traffic may explain the trends in fractal dimension and aggregate fraction. During the morning, aggregates are relatively abundant, because many automobiles and a few trucks are emitting them. As the total (truck and automobile) traffic decreases, aggregates become less

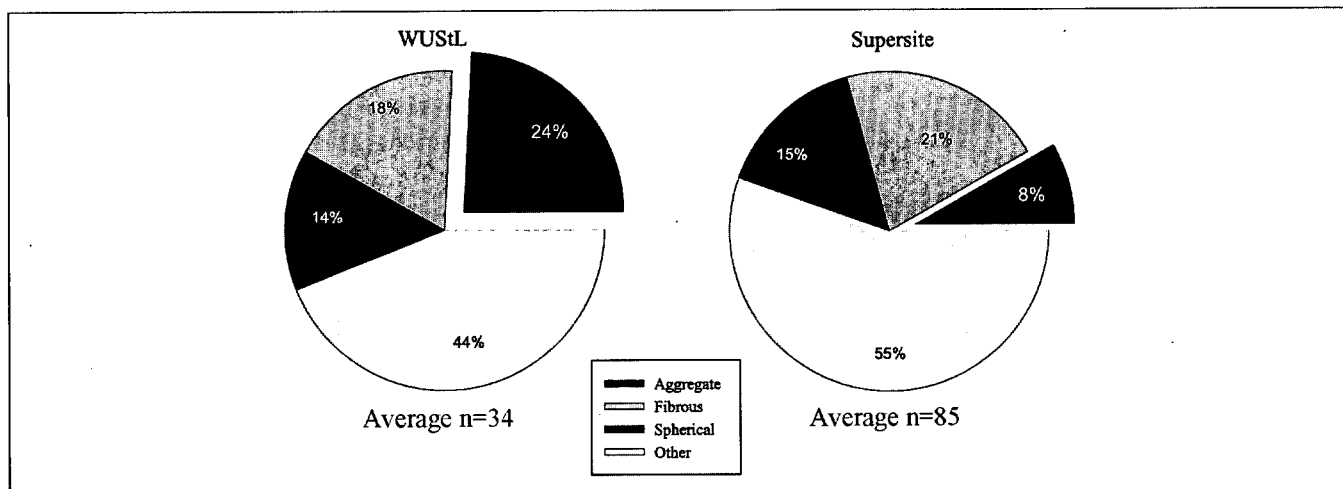


**Figure 6.** Average composition and number of particles collected every 2 hr at WUSTL (3:00–5:00 p.m.) and at the Supersite (7:00 a.m.–7:00 p.m.). While the Supersite had a higher concentration of particles, a lower fraction of those were aggregates.

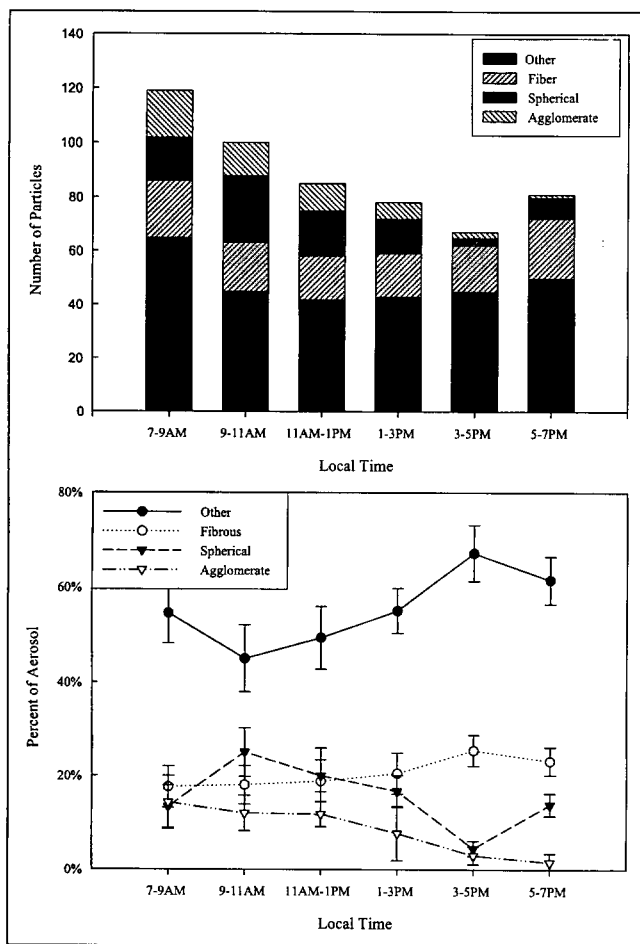


**Figure 7.** (A) Absolute number of particles found on four TEM grid squares at the Supersite vs. local time; (B) aerosol composition at the Supersite over time. Error bars represent the standard error within each sample.

abundant. However, the aggregates that are emitted are increasingly from trucks and have a lower fractal dimension. This leads to the observed lower characteristic  $D_f$  as well as the lower fraction of aggregates. Other aerosol measurements, such as particle size distributions and black carbon concentrations, would help differentiate between the two scenarios.

## CONCLUSIONS

A pilot study was conducted to demonstrate the viability of establishing the shape and fractal dimension of ambient  $PM_{2.5}$ . An electrostatic aerosol sampler was demonstrated to be a practical method to collect ambient PM directly on electron microscopy grids for morphology determination. The unit could be readily incorporated into existing  $PM_{2.5}$  samplers. After an image was obtained from the SEM, a computer program was used to establish the fractal dimension of each aggregate and the average fractal dimension for each aerosol sample.

The system was used to examine the morphology of ambient  $PM_{2.5}$  at two locations in St. Louis. Aggregates at the two sites had fractal dimensions that were not significantly different. However, the shape distributions of the aerosols were different. The WUSTL location had a higher aggregate fraction and number and a lower fraction in the "other" category than did the Supersite. Both morphological composition and fractal dimensions showed differences as the day progressed at the Supersite. While fractal dimensions of the aggregates have been reported extensively in the paper, eq 3 was not used to report values of the surface area of the aggregates. In general, smaller fractal dimensions would imply a higher surface area,

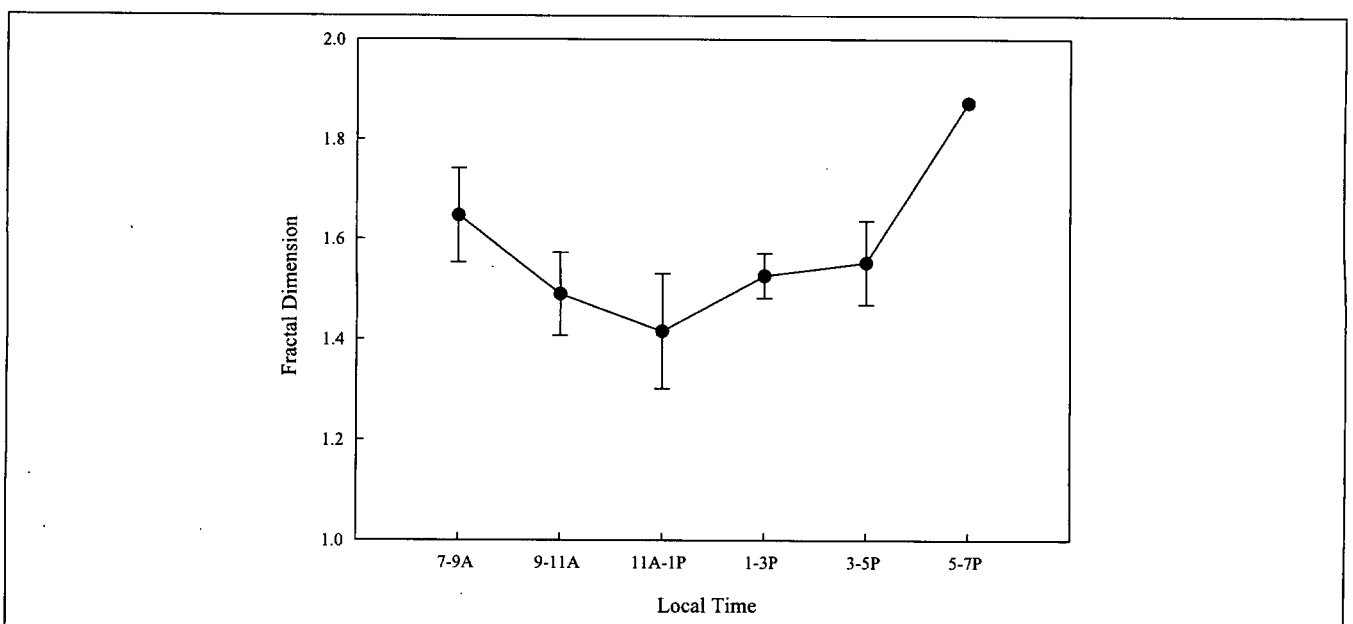


**Figure 8.** Variation in the calculated two-dimensional fractal dimension over 12 hr for the Supersite samples. Error bars represent 1 SD within each sample.

provided the number of primary particles was similar. Thus, at times of the day or at locations where smaller fractal dimension aggregates are encountered, the surface area of the aggregated particles also is higher.

The fractal dimension alone cannot be relied upon to describe adequately the morphology of an aerosol. This is especially true when the portion of the aerosol examined for fractal dimension is small or unknown, or if the aggregates are composed of very few primary particles. Other metrics for describing the morphology of the aerosol must be employed to effectively discern differences in the shapes of two different aerosols or even the same aerosol at different times.

In this study, as well as in other research,<sup>10</sup> the shape distribution was used as another metric for morphological description. While there was small variation in fractal dimension, larger variations in the aerosol shape distribution were observed. As such, it is proposed that the shape distribution is also a valuable tool for describing an aerosol. Detailed studies are under way in the greater Cincinnati airshed to evaluate trends in morphology (fractal dimension and shape distribution) as a function of the distance from a highway, to help determine the impact that diesel trucks play on ambient aerosol morphology.

## ACKNOWLEDGMENTS

The authors gratefully acknowledge the support provided by the National Institutes of Environmental Health Sciences (Grant # RO1 ES11170). Rafael McDonald also acknowledges the partial support provided by a Henry J. Schwartz Jr. scholarship. The authors also thank the EPA Supersite in St. Louis for access to and help at their site.

## REFERENCES

- Dab, W.; Segala, C.; Dor, F.; Festy, B.; Lameloise, P.; Le Moullec, Y.; Le Tertre, A.; Medina, S.; Quenel, P.; Wallaert, B.; Zmirou, D. Air Pollution and Health: Correlation or Causality? The Case of the Relationship between Exposure to Particles and Cardiopulmonary Mortality; *J. Air & Waste Manage. Assoc.* **2001**, *51*, 220-235.
- Oberdorster, G.; Ferin, J.; Gelein, R.; Cox, C.; Baggs, R.; Morrow, P. Increased Pulmonary Toxicity of Inhaled Ultrafine Particles: Due to Lung Overload Alone?; *Ann. Occup. Hyg.* **1994**, *38*, 295-302.
- Oberdorster, G.; Gelein, R.M.; Ferin, J.; Weiss, B. Association of Particulate Air Pollution and Acute Mortality: Involvement of Ultrafine Particles?; *Inhal. Toxicol.* **1995**, *7*, 111-124.
- Schwartz, J.; Dockery, D. Particulate Air Pollution and Daily Mortality in Steubenville, OH; *Am. J. Epidemiol.* **1992**, *125*, 12-19.
- Schwartz, J.; Dockery, D. Increased Mortality in Philadelphia Associated with Daily Air Pollution Concentrations; *Am. Rev. Respir. Dis.* **1992**, *145*, 600-604.
- McMurry, P.H.; Woo, K.S. Size Distributions of 3-100 nm Urban Atlanta Aerosols: Measurement and Observations; *J. Aerosol Med.* **2002**, *15*, 169-178.
- Lee, T.G. Ph.D. Thesis, University of Cincinnati, Ohio, 1999.
- Rogak, S.N.; Flagan, R.; Nguyen, H. The Mobility and Structure of Aerosol Agglomerates; *Aerosol Sci. Technol.* **1993**, *18*, 25-47.
- Katrinak, K.A.; Rez, P.; Perkes, P.R.; Buseck, P.R. Fractal Geometry of Carbonaceous Aggregates from an Urban Aerosol; *Environ. Sci. Technol.* **1993**, *27*, 239-247.

- Ebert, M.; Weinbruch, S.; Rausch, A.; Gorzawski, G.; Helas, G.; Hoffman, P.; Wex, H. Complex Refractive Index of Aerosols during LACE 98 as Derived from the Analysis of Individual Particles; *J. Geophys. Res.* **2002**, *107*, 1-15.
- Kindratenko, V.; Van Espen, P.; Treiger, B.; Van Grieken, R. Fractal Dimension Classification of Aerosol Particles by Computer-Controlled Scanning Electron Microscopy; *Environ. Sci. Technol.* **1994**, *28*, 2197-2202.
- Cai, J.; Lu, N.; Sorenson, C. Comparison of Size and Morphology of Soot Aggregates as Determined by Light Scattering and Electron Microscope Analysis; *Langmuir* **1993**, *9*, 2861-2867.
- Liu, B.; Srinivasachar, S.; Helble, J. The Effect of Chemical Composition on the Fractal-Like Structure of Combustion Generated Inorganic Aerosols; *Aerosol Sci. Technol.* **2001**, *33*, 459-469.
- Xiong, C.; Friedlander, S.K. Morphological Properties of Atmospheric Aerosol Aggregates; *Proc. Nat. Acad. Sci.* **2001**, *98*, 11851-11856.
- Dye, A.L.; Rhead, M.M.; Trier, C.J. The Quantitative Morphology of Roadside and Background Urban Aerosol in Plymouth, UK; *Atmos. Environ.* **2000**, *34*, 3139-3148.
- Bonczyk, P.A.; Sangiovanni, J.J. Optical and Probe Measurements of Soot in a Burning Fuel Droplet Stream; *Combust. Sci. Technol.* **1984**, *36*, 135-147.
- Friedlander, S.K. *Smoke Dust and Haze: Fundamentals of Aerosol Dynamics*; Oxford University Press: New York, NY, 2000.
- Mandelbrot, B. *The Fractal Geometry of Nature*; W.H. Freeman: San Francisco, CA, 1982.
- Ebert, M.; Inerle-Hof, M.; Weinbruch, S. Environmental Scanning Electron Microscopy as a New Technique to Determine the Hygroscopic Behaviour of Individual Aerosol Particles; *Atmos. Environ.* **2002**, *36*, 5909-5916.
- Forrest, S.; Witten, T. Long-Range Correlations in Smoke-Particle Aggregates; *J. Phys. A: Math. Gen.* **1979**, *12*, L109-L117.
- Samson, R.J.; Mulholland, G.W.; Gentry, J.W. Structural Analysis of Soot Agglomerates; *Langmuir* **1987**, *3*, 272-281.
- Huang, P.F.; Turpin, B.J.; Pihlo, M.J.; Kittleson, D.B.; McMurry, P.H. Effects of Water Condensation and Evaporation on Diesel Chain-Agglomerate Morphology; *J. Aerosol Sci.* **1994**, *25*, 447-459.
- Yang, G.; Biswas, P. Computer Simulation of the Aggregation and Sintering Restructuring of Fractal-Like Clusters Containing Limited Numbers of Primary Particles; *J. Colloid Interface Sci.* **1999**, *211*, 142-150.
- Scion Image; Scion Corporation: Frederick, MD, 2002.
- Kumar, P.; Biswas, P. *Matlab Program to Evaluate Fractal Dimensions*; Washington University in St. Louis Aerosol and Air Quality Research Lab: St. Louis, MO, 2001. Available at: [www.aerosols.wustl.edu/aaqrl](http://www.aerosols.wustl.edu/aaqrl).
- ImageJ v1.30h; National Institutes of Health: Atlanta, GA, 2002. Available at: <http://rsb.info.nih.gov/ij/>.
- Baron, P.A. *Aerosol Calculator Program*; Freeware, 2001. Available at: [www.tsi.com/particle/downloads/software/software.htm](http://www.tsi.com/particle/downloads/software/software.htm).
- Chen, D.-R. Washington University in St. Louis, MO. Personal Communication. Electrostatic Losses in Tubing, February 10, 2004.
- Hinds, W.C. *Aerosol Technology: Properties, Behavior, and Measurement of Airborne Particles*; J. Wiley and Sons: New York, 1999.
- Model 3100 Electrostatic Aerosol Sampler Instruction Manual Revision A; TSI Inc.: St. Paul, MN, 1988.
- Liu, B.Y.H.; Whitby, K.T.; Yu, H.S. Electrostatic Aerosol Sampler for Light and Electron Microscopy; *Rev. Sci. Instr.* **1967**, *38*, 100-102.

### About the Authors

Rafael McDonald is currently a doctoral student at Washington University in St. Louis. Dr. Pratim Biswas is the Stifel and Quinette Jens Professor of Environmental Engineering and the director of the Environmental Engineering Science Program at Washington University in St. Louis, St. Louis, MO. Address correspondence to: Pratim Biswas, Environmental Engineering Science, Washington University in St. Louis, One Brookings Drive, Campus Box 1180, St. Louis, MO 63130; phone: 314-935-5482; fax: 314-935-4338, e-mail: [pratim.biswas@seas.wustl.edu](mailto:pratim.biswas@seas.wustl.edu).

A vertical bar on the left side of the page, consisting of a series of horizontal segments in shades of yellow and orange, with a small red diamond at the top.

COPYRIGHT INFORMATION

TITLE: A Methodology to Establish the Morphology of Ambient Aerosols

SOURCE: J Air Waste Manage Assoc (1995) 54 no9 S 2004

WN: 0425205991005

The magazine publisher is the copyright holder of this article and it is reproduced with permission. Further reproduction of this article in violation of the copyright is prohibited. To contact the publisher:

<http://www.awma.org/>

Copyright 1982-2004 The H.W. Wilson Company. All rights reserved.